















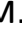









Search for $B_s^0 \rightarrow \ell^\mp \tau^\pm$ with the Semi-leptonic Tagging Method at Belle

The Belle Collaboration

L. Nayak , S. Nishida , A. Giri , I. Adachi , H. Aihara , D. M. Asner ,
H. Atmacan , V. Aulchenko , T. Aushev , R. Ayad , V. Babu ,
S. Bahinipati , Sw. Banerjee , M. Bauer , P. Behera , K. Belous ,
J. Bennett , M. Bessner , B. Bhuyan , D. Biswas , D. Bodrov ,
J. Borah , A. Bozek , M. Bračko , P. Branchini , T. E. Browder ,
A. Budano , M. Campajola , D. Červenkov , M.-C. Chang ,
B. G. Cheon , K. Chilikin , H. E. Cho , K. Cho , S.-K. Choi ,
Y. Choi , S. Choudhury , D. Cinabro , J. Cochran , S. Das ,
N. Dash , G. De Nardo , G. De Pietro , R. Dhamija , F. Di Capua ,
J. Dingfelder , Z. Doležal , T. V. Dong , D. Dossett , S. Dubey ,
D. Epifanov , T. Ferber , D. Ferlewicz , B. G. Fulsom , R. Garg ,
V. Gaur , P. Goldenzweig , E. Graziani , T. Gu , Y. Guan , S. Halder ,
T. Hara , K. Hayasaka , H. Hayashii , M. T. Hedges , D. Herrmann ,
W.-S. Hou , C.-L. Hsu , T. Iijima , K. Inami , G. Inguglia , N. Ipsita ,
A. Ishikawa , R. Itoh , M. Iwasaki , W. W. Jacobs , E.-J. Jang ,
S. Jia , Y. Jin , K. K. Joo , A. B. Kaliyar , T. Kawasaki , C. Kiesling ,
C. H. Kim , D. Y. Kim , K.-H. Kim , Y.-K. Kim , K. Kinoshita ,
P. Kodyš , T. Konno , A. Korobov , S. Korpar , E. Kovalenko ,
P. Krizan , P. Krokovny , T. Kuhr , M. Kumar , R. Kumar ,
K. Kumara , A. Kuzmin , Y.-J. Kwon , S. C. Lee , J. Li , L. K. Li ,
Y. Li , J. Libby , K. Lieret , Y.-R. Lin , D. Liventsev , T. Luo ,
Y. Ma , M. Masuda , T. Matsuda , S. K. Maurya , F. Meier ,
M. Merola , F. Metzner , K. Miyabayashi , R. Mizuk , G. B. Mohanty ,
I. Nakamura , M. Nakao , Z. Natkaniec , A. Natochii , N. K. Nisar ,
S. Ogawa , H. Ono , P. Oskina , P. Pakhlov , G. Pakhlova , T. Pang ,
S. Pardi , J. Park , S.-H. Park , A. Passeri , S. Paul , T. K. Pedlar ,
R. Pestotnik , L. E. Piilonen , T. Podobnik , E. Prencipe ,
M. T. Prim , A. Rostomyan , N. Rout , G. Russo , S. Sandilya ,
A. Sangal , L. Santelj , V. Savinov , G. Schnell , C. Schwanda

A. J. Schwartz , Y. Seino , K. Senyo , M. E. Sevior , M. Shapkin ,
C. Sharma , J.-G. Shiu , A. Sibidanov , E. Solovieva , M. Starič ,
M. Sumihama , T. Sumiyoshi , M. Takizawa , K. Tanida ,
F. Tenchini , K. Trabelsi , M. Uchida , Y. Unno , K. Uno , S. Uno ,
P. Urquijo , S. E. Vahsen , G. Varner , K. E. Varvell , A. Vinokurova ,
D. Wang , M.-Z. Wang , S. Watanuki , E. Won , B. D. Yabsley ,
W. Yan , J. Yelton , Y. Yook , C. Z. Yuan , L. Yuan , Y. Yusa ,
Y. Zhai , Z. P. Zhang , V. Zhilich , V. Zhukova 

E-mail: lopamudra.nayakcda@gmail.com, shohei.nishida@kek.jp,
giria@phy.iith.ac.in

ABSTRACT: We present a search for the lepton-flavor-violating decays $B_s^0 \rightarrow \ell^\mp \tau^\pm$, where $\ell = e, \mu$, using the full data sample of 121 fb^{-1} collected at the $\Upsilon(5S)$ resonance with the Belle detector at the KEKB asymmetric-energy e^+e^- collider. We use $B_s^0 \bar{B}_s^0$ events in which one B_s^0 meson is reconstructed in a semileptonic decay mode and the other in the signal mode. We find no evidence for $B_s^0 \rightarrow \ell^\mp \tau^\pm$ decays and set upper limits on their branching fractions at 90% confidence level as $\mathcal{B}(B_s^0 \rightarrow e^\mp \tau^\pm) < 14.1 \times 10^{-4}$ and $\mathcal{B}(B_s^0 \rightarrow \mu^\mp \tau^\pm) < 7.3 \times 10^{-4}$. Our result represents the first upper limit on the $B_s^0 \rightarrow e^\mp \tau^\pm$ decay rate.

KEYWORDS: LFV, Belle, KEKB

Contents

1	Introduction	1
2	Data sample and Belle detector	2
3	Event Selection and Analysis Overview	2
4	Systematic Uncertainties	7
5	Results and Summary	9

1 Introduction

The lepton-flavor-violating (LFV) decays $B_s^0 \rightarrow \ell^\mp \tau^\pm$, where $\ell = e, \mu$, are forbidden in the standard model (SM). Such decays can occur via neutrino mixing by loop and box diagrams [1], but the predicted decay rates are far below current experimental capabilities. Thus, any observations at current experiments would constitute an unambiguous signature of new physics (NP). Recent results indicating possible lepton flavor universality violation in B meson decay have been discussed in Refs. [2, 3], where many NP models are proposed to explain it. Such models allow significantly enhanced LFV decay rates that may be detectable with current facilities. For example, the models containing a heavy neutral gauge boson (Z') could lead to an enhanced $B_s^0 \rightarrow \mu^- \tau^+$ branching fraction, up to 10^{-8} when only left- or right-handed couplings to quarks are considered, or of order 10^{-6} [4] if both are allowed. In models with either scalar or vector leptoquarks, the largest prediction for the $B_s^0 \rightarrow \ell^- \tau^+$ branching fraction ranges from 10^{-10} to 10^{-5} [5, 6], depending on the assumed leptoquark mass. It is imperative to search for signals of physics beyond the SM in all possible avenues, and since the expected branching fraction of $B_s^0 \rightarrow e^- \tau^+$ may differ from $B_s^0 \rightarrow \mu^- \tau^+$ depending on models, it is important to search for both decay modes to obtain additional information regarding the NP.

To date, no experimental results for $B_s^0 \rightarrow e^\mp \tau^\pm$ have been reported while an upper limit $\mathcal{B}(B_s^0 \rightarrow \mu^\mp \tau^\pm) < 3.4 \times 10^{-5}$ at 90% confidence level (CL) [7] has been reported by LHCb.

In this paper, we report a search for $B_s^0 \rightarrow \ell^\mp \tau^\pm$ decays using 121 fb^{-1} of data collected by the Belle experiment at the KEKB asymmetric-energy e^+e^- collider [8, 9]. The data were collected at an e^+e^- center-of-mass (c.m.) energy corresponding to the $\Upsilon(5S)$ resonance mass.

2 Data sample and Belle detector

The Belle detector is a large-solid-angle magnetic spectrometer comprising a silicon vertex detector, a 50-layer central drift chamber (CDC), an array of aerogel threshold Cherenkov counters (ACC), a barrel-like arrangement of time-of-flight scintillation counters (TOF), and a CsI(Tl) crystal electromagnetic calorimeter (ECL). All these components are located inside a superconducting solenoid providing a magnetic field of 1.5 T. An iron flux return located outside the solenoid coil is instrumented with resistive plate chambers to detect K_L^0 mesons and muons (KLM). A more detailed description of the detector and its layout and performance can be found in Refs. [10, 11].

We study the properties of signal events, identify sources of background, and optimize selection criteria using Monte Carlo (MC) simulated events. These samples are generated using EvtGen [12]. The detector response is simulated using the Geant3 framework [13]. We simulate 20 million $B_s^0 \rightarrow \ell^\mp \tau^\pm$ MC events to study the detector response and to calculate signal reconstruction efficiencies. To estimate backgrounds, we use MC samples of $B_s^{(*)} \bar{B}_s^{(*)}$ and $B_{u,d}^{(*)} \bar{B}_{u,d}^{(*)} X$ events, and $e^+e^- \rightarrow q\bar{q}$ ($q = u, d, s, c$) events. These samples, referred to as generic MC, are equivalent to six times the data luminosity. The Belle data are converted into the Belle II format [14], and the particle and event reconstruction are performed within the basf2 framework [15, 16] of the Belle II experiment.

The B_s^0 and \bar{B}_s^0 mesons are produced in the process $e^+e^- \rightarrow \Upsilon(5S) \rightarrow B_s^{(*)0} \bar{B}_s^{(*)0}$, with $B_s^{*0} \rightarrow B_s^0 \gamma$, $\bar{B}_s^{*0} \rightarrow \bar{B}_s^0 \gamma$ and with 100% mixing for $B_s^0 \leftrightarrow \bar{B}_s^0$. The $\Upsilon(5S)$ resonance production cross section is 340 ± 16 pb [17], and f_s , its total branching fraction for decays to $B_s^{(*)0} \bar{B}_s^{(*)0}$, is 0.201 ± 0.031 [18]. Therefore, the Belle data sample is estimated to contain $(16.6 \pm 2.7) \times 10^6$ B_s mesons.

3 Event Selection and Analysis Overview

Hereafter, B_s refers to either B_s^0 or \bar{B}_s^0 , and the inclusion of charge-conjugated modes is implied. In this analysis, one B_s is reconstructed in a semileptonic decay mode $\bar{B}_s^0 \rightarrow D_s^+ \ell^- (X) \bar{\nu}_\ell$ and used as a tag, where X stands for any particles such as π or $\pi\pi$, and the signal $B_s \rightarrow \ell^- \tau^+$ is searched for in the mode $\tau^+ \rightarrow \ell^+ \bar{\nu}_\tau \nu_\ell$. We label the primary and secondary leptons from the τ decay on the signal side B_s as ℓ_1 and ℓ_2 , and the lepton on the tag side as ℓ_3 . In short, we search for $B_s \rightarrow \ell_1^- \tau^+ (\rightarrow \ell_2^+ \bar{\nu}_\tau \nu_{\ell_2})$ with \bar{B}_s^0 tagged by the decay $\bar{B}_s^0 \rightarrow D_s^+ \ell_3^- (X) \bar{\nu}_{\ell_3}$. Figure 1 shows a schematic diagram of the process, separated into signal and tag sides. To avoid biasing the results, all selection criteria are determined in a ‘‘blind’’ manner, i.e., they are optimized using MC samples only, before the experimental data in the signal region are revealed.

For charged particles, aside for those from K_S^0 , the distance of nearest approach of the track perpendicular to and along the beam direction, with respect to the

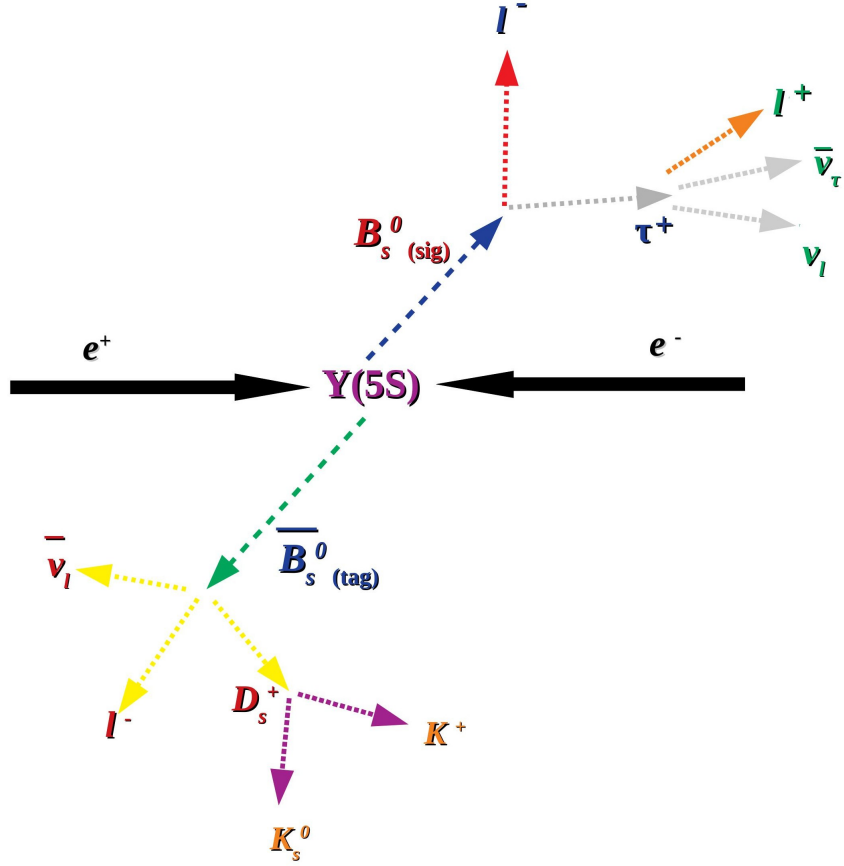


Figure 1: A schematic diagram of the process under study, separated into signal and tag sides.

nominal interaction point, are required to be less than 0.5 cm and 2.0 cm, respectively. The K_s^0 candidates are reconstructed by combining two oppositely charged particles (assumed to be pions) with an invariant mass between 487 and 508 MeV/c^2 ; this corresponds to window of approximately $\pm 3\sigma$ of around the nominal K_s^0 mass [18]. Such candidates are further subjected to a neural network-based identification [19]. The π^0 candidates are reconstructed from pairs of photons detected as ECL clusters without any associated charged tracks in the CDC. The energy of each photon is required to be greater than 50 MeV if the photon is detected in the barrel region ($32.2^\circ < \theta < 128.7^\circ$, where θ is its polar angle), greater than 100 MeV if the photon is in the forward endcap region ($12.4^\circ < \theta < 31.4^\circ$), and greater than 150 MeV if the photon is in the backward endcap region ($130.7^\circ < \theta < 155.1^\circ$) [10, 11]. The invariant mass of each photon pair is required to be between 120 and 150 MeV/c^2 ; this

corresponds to window of approximately $\pm 3\sigma$ in resolution around the nominal π^0 mass, and the reconstructed π^0 momentum in the c.m. frame ($p_{\pi^0}^*$) must be greater than 0.2 GeV/c. A mass constrained fit to the nominal π^0 mass is performed to improve momentum resolution.

To identify charged hadrons, we use information on the light yield from the ACC, timing from the TOF, and specific ionization from the CDC. This information is combined into likelihoods \mathcal{L}_K and \mathcal{L}_π for a given track to be a K^+ or π^+ , respectively. To identify K^+ or π^+ tracks, we require $\mathcal{L}_K/(\mathcal{L}_K + \mathcal{L}_\pi) > 0.6$ or $\mathcal{L}_\pi/(\mathcal{L}_K + \mathcal{L}_\pi) > 0.6$. This requirement is more than 93% efficient in identifying pions, with a K^+ mis-identification rate below 5%. Muon candidates are selected based on information from the KLM [20]. We calculate a normalized muon likelihood ratio $\mathcal{R}_\mu = \mathcal{L}_\mu/(\mathcal{L}_\mu + \mathcal{L}_\pi + \mathcal{L}_K)$, where \mathcal{L}_μ is the likelihood for muons, and require $\mathcal{R}_\mu > 0.9$. This requirement has an efficiency of 85 – 92% and a probability of misidentifying a hadron as a muon below 7%. Electron candidates are identified using the ratio of calorimetric cluster energy to particle momentum, the shower shape in the ECL, the matching of the track with the ECL cluster, the specific ionization in the CDC, and the number of photoelectrons in the ACC [21]. This information is used to calculate a normalized electron likelihood ratio $\mathcal{R}_e = \mathcal{L}_e/(\mathcal{L}_e + \mathcal{L}_{\text{had}})$, where \mathcal{L}_e is the likelihood for electrons and \mathcal{L}_{had} is a product of hadron likelihoods. We require $\mathcal{R}_e > 0.9$. This requirement has an efficiency of 84 – 92% and a probability of misidentifying a hadron as an electron below 1%.

For the signal side $B_s \rightarrow \ell_1^- \tau^+ (\rightarrow \ell_2^+ \bar{\nu}_\tau \nu_{\ell_2})$, we require that the two leptons ℓ_1 and ℓ_2 have opposite charges and that $p_1^* > p_2^*$, $p_1^* > p_3^*$, and $p_1^* > 1.9$ GeV/c, where p_1^* , p_2^* and p_3^* are the momenta of ℓ_1 , ℓ_2 and ℓ_3 in the c.m. frame. To suppress background coming from $J/\psi \rightarrow \ell^+ \ell^-$, the candidate is rejected if the invariant mass of the two leptons $M_{\ell_1 \ell_2}$ satisfies $M_{\ell_1 \ell_2} \in [3.01, 3.12]$ GeV/c² for the $B_s \rightarrow e^- \tau^+ (\rightarrow e^+ \bar{\nu}_\tau \nu_e)$ mode, and $M_{\ell_1 \ell_2} \in [3.05, 3.12]$ GeV/c² for the $B_s \rightarrow \mu^- \tau^+ (\rightarrow \mu^+ \bar{\nu}_\tau \nu_\mu)$ mode. The wider asymmetric veto interval for the electron mode is due to bremsstrahlung energy loss.

For the tag side $\bar{B}_s^0 \rightarrow D_s^+ \ell_3^- (X) \bar{\nu}_{\ell_3}$, the charge of ℓ_3 can be opposite to or the same as ℓ_1 , as B_s mixing produces equal numbers of opposite and same charge combinations. However, we accept only combinations where the charges of ℓ_1 and ℓ_3 are the same; this significantly reduces combinatorial background. We reconstruct D_s meson candidates with opposite charge to ℓ_3 from the following five decay modes: $D_s^+ \rightarrow \phi \pi^+$, $\bar{K}^{*0} K^+$, $\phi \rho^0 \pi^+$, $K_S^0 K^+$ and $\phi \rho^+$. Here, ρ^0 , ρ^+ , \bar{K}^{*0} and ϕ are reconstructed through $\rho^0 \rightarrow \pi^+ \pi^-$, $\rho^+ \rightarrow \pi^+ \pi^0$, $\bar{K}^{*0} \rightarrow K^- \pi^+$ and $\phi \rightarrow K^+ K^-$, and candidates are required to have a reconstructed invariant mass $625 \text{ MeV}/c^2 < M_{\pi^+ \pi^- (\pi^+ \pi^0)} < 925 \text{ MeV}/c^2$ for $\rho^0 (\rho^+)$, $845 \text{ MeV}/c^2 < M_{K^+ \pi^-} < 945 \text{ MeV}/c^2$ for \bar{K}^{*0} , and $1.01 \text{ GeV}/c^2 < M_{K^+ K^-} < 1.03 \text{ GeV}/c^2$ for ϕ . The D_s candidate is then combined with an e or μ to form a B_s meson candidate. Figure 2 shows the mass distribution of D_s^+ meson candidates. The mass of the D_s^+ candidate is required

to be between 1.96 and 1.98 GeV/c^2 . These mass windows correspond to $\pm 3\sigma$ in resolution around the nominal masses [18]. Figure 3 shows the p_1^* distribution for $B_s \rightarrow e^- \tau^+$ and $B_s \rightarrow \mu^- \tau^+$ after initial selections.

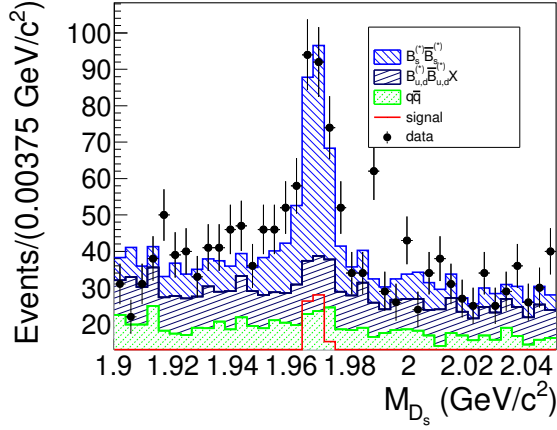


Figure 2: The M_{D_s} distribution of signal MC, generic MC and data. The different background component in generic MC are indicated by different colours as shown in the legend. The MC samples are normalized with respect to the data luminosity. The signal components correspond to $\mathcal{B} = 1 \times 10^{-2}$.

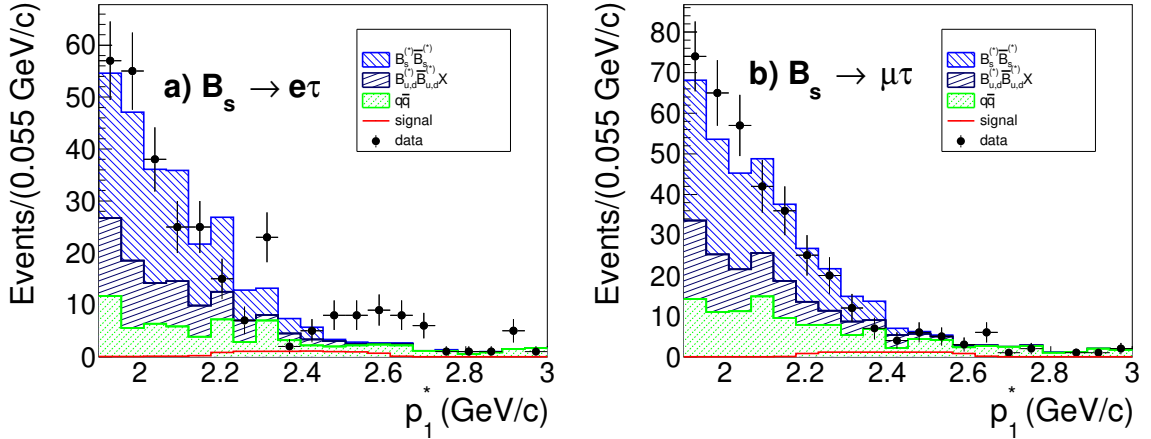


Figure 3: The p_1^* distribution of signal MC, generic MC and data in $B_s \rightarrow e^- \tau^+$ (a) and $B_s \rightarrow \mu^- \tau^+$ (b) modes. The different background components in generic MC are indicated by different colours as shown in the legend. The MC samples are normalized with respect to the data luminosity. The signal components correspond to $\mathcal{B} = 1 \times 10^{-3}$.

The background comes from the continuum $e^+e^- \rightarrow q\bar{q}$ process and $e^+e^- \rightarrow B_s^{(*)0}\bar{B}_s^{(*)0}, B^{(*)}\bar{B}^{(*)}X$. The continuum events have final-state particles momenta spatially correlated in two directions forming jet-like structures, while particles from $B_s^{(*)0}\bar{B}_s^{(*)0}$ events are distributed almost uniformly over the full solid angle in the c.m. frame. We use this difference in the topology to suppress the continuum background. The background from $B_s^{(*)0}\bar{B}_s^{(*)0}$ or $B^{(*)}\bar{B}^{(*)}X$ are suppressed using other variables characterizing the signal decay chains. We form a single FastBDT [22] classifier trained using simulated samples with the following discriminating variables as input: p_2^* ; p_3^* ; the extra energy from the tracks and clusters not used for signal and tag reconstruction in the calorimeter; the sum of the energy of the clusters and charged tracks in the c.m. frame; the missing energy which is the absolute value of the sum of the four-momenta of all charged candidates; the invariant mass squared of the missing momentum; $(2E_{\text{beam}}^*E_{D_s\ell_3}^* - m_{B_s}^2c^4 - M_{D_s\ell_3}^2c^4)/(2|\vec{p}_{B_s}^*||\vec{p}_{D_s\ell_3}^*|c^2)$; the cosine of the angle between p_1^* and p_2^* ; the mass of the D_s^+ candidate; and 16 modified Fox-Wolfram moments [23, 24] calculated from the signal B_s daughters and the particles from the rest of the event. Here, E_{beam}^* is the beam energy in the c.m. frame, m_{B_s} is the nominal B_s mass, $|\vec{p}_{B_s}^*| = \left(\sqrt{E_{\text{beam}}^{*2} - m_{B_s}^2c^2}\right)/c$, and $E_{D_s\ell_3}^*$, $\vec{p}_{D_s\ell_3}^*$ and $M_{D_s\ell_3}$ are calculated from the reconstructed $D_s\ell_3$ system.

These variables do not have a significant correlation with the signal extraction variable p_1^* . The FastBDT classifier output $\mathcal{O}_{\text{FastBDT}}$ ranges from zero, where background events peak, to one, where signal events peak. For each signal mode, we

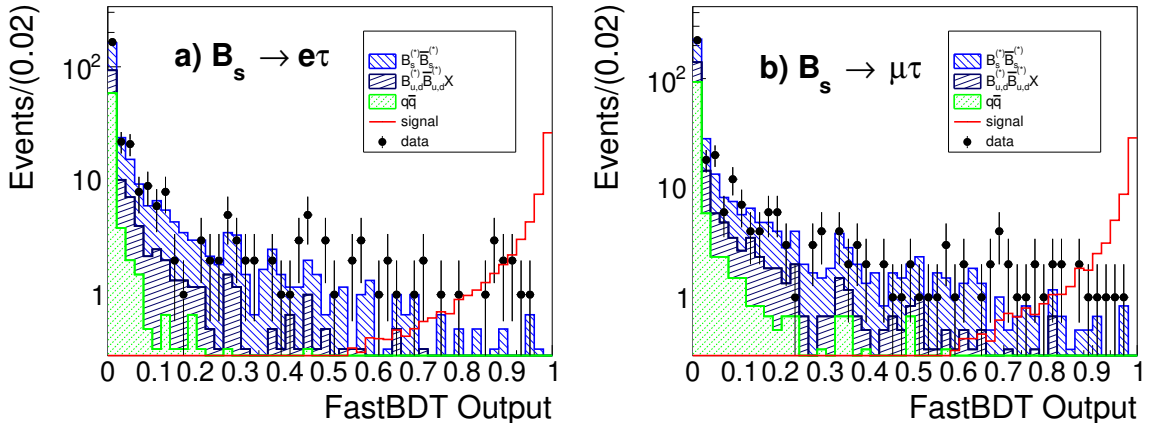


Figure 4: The $\mathcal{O}_{\text{FastBDT}}$ distribution of signal MC, generic MC and data in $B_s \rightarrow e^- \tau^+$ (a) and $B_s \rightarrow \mu^- \tau^+$ (b) modes. The different background components in generic MC are indicated by different colours as shown in the legend. The MC samples are normalized with respect to the data luminosity. The signal components correspond to $\mathcal{B} = 1 \times 10^{-2}$. The distributions are shown on a logarithmic scale.

choose selection criteria on $\mathcal{O}_{\text{FastBDT}}$ that optimize a figure-of-merit (FOM) [25]. The FOM is defined as $\epsilon_{\text{sig}}/[(a/2) + \sqrt{N_B}]$, where $a = 3$, ϵ_{sig} is the reconstruction efficiency of signal events as determined from MC simulation, and N_B is the number of background events expected within the signal region of $p_1^* \in [2.1, 2.7]$ GeV/ c . Figure 4 shows the FastBDT output distributions. Based on FOM studies, we require $\mathcal{O}_{\text{FastBDT}} > 0.90$ for $B_s \rightarrow e^- \tau^+$ and $\mathcal{O}_{\text{FastBDT}} > 0.94$ for $B_s \rightarrow \mu^- \tau^+$ modes. These criteria reject 98% of the background events with 40% signal loss. After applying all selection criteria, 8-9% of events have multiple signal candidates. For these events, the candidate with the highest FastBDT output is retained. This criterion is found to select the correct signal candidate 91% of the time for both decay modes. The reconstruction efficiencies from the signal simulations are 0.032% and 0.031% for $B_s \rightarrow e^- \tau^+$ and $B_s \rightarrow \mu^- \tau^+$, respectively. Figure 5 shows the p_1^* distribution after applying the selection on $\mathcal{O}_{\text{FastBDT}}$. We observe three events for $B_s \rightarrow e^- \tau^+$ and one event for $B_s \rightarrow \mu^- \tau^+$.

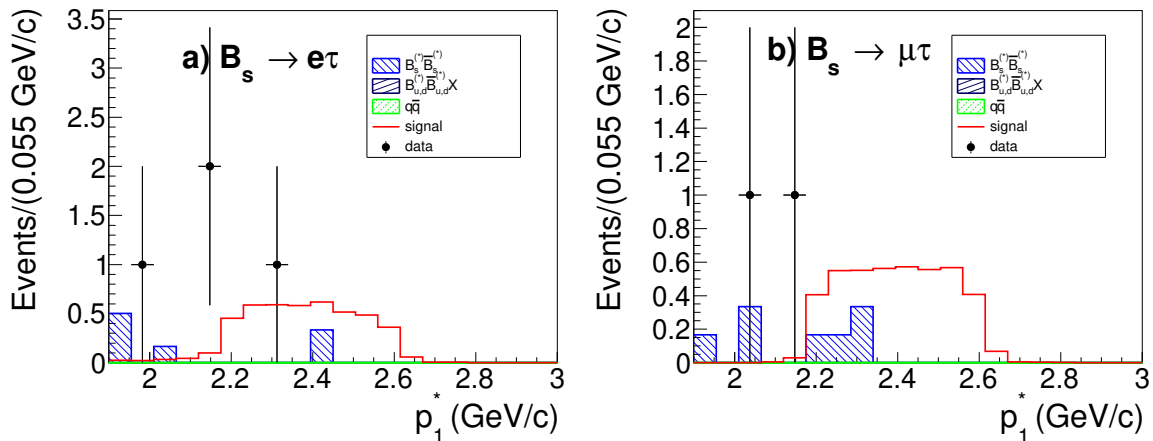


Figure 5: The p_1^* distribution of signal MC, generic MC and data in (a) $B_s \rightarrow e^- \tau^+$ and (b) $B_s \rightarrow \mu^- \tau^+$ modes. The different background components in generic MC are indicated by different colours as shown in the legend. The MC samples are normalized with respect to the data luminosity. The signal components correspond to $\mathcal{B} = 1 \times 10^{-3}$.

4 Systematic Uncertainties

A summary of systematic uncertainties is shown in Table 1. In order to estimate the systematic uncertainty of the $\mathcal{O}_{\text{FastBDT}}$ selection, we use 711 fb $^{-1}$ data sample taken at the $\Upsilon(4S)$ and reconstruct $B^- \rightarrow D^0 \pi^-$ decays, tagging the other side B^+ by $B^+ \rightarrow \bar{D}^0 \ell^+ \nu$. Here, the signal side D^0 is reconstructed in the mode $K^- \pi^+$, while

the tag side \bar{D}^0 is reconstructed in the three decay modes $\bar{D}^0 \rightarrow K^+\pi^-$, $K_S^0\pi^+\pi^-$, and $K^+\pi^-\pi^+\pi^-$. In this study, π^- from B^- is treated as ℓ_1 in the signal mode, K^- from D^0 as ℓ_2 , and π^+ from D^0 is neglected. With these changes, the topology of these events becomes similar to our signal mode, and we use the same MVA as for the signal without retraining. For this control sample study, we apply $M_{D^0} \in [1.85, 1.88]$ GeV/ c^2 for both the D^0 in the signal side and \bar{D}^0 in the tag side, $|\Delta E| < 0.05$ GeV and $M_{bc} > 5.2$ GeV/ c^2 . Here, M_{bc} and ΔE are defined by $M_{bc} = (\sqrt{E_{\text{beam}}^{*2} - |\vec{p}_B^*|^2 c^2})/c^2$ and $\Delta E = E_B^* - E_{\text{beam}}^*$, where E_B^* and \vec{p}_B^* are the energy and momentum of the reconstructed B meson in the c.m. frame. We extract the signals from a fit to M_{bc} with and without the $\mathcal{O}_{\text{FastBDT}}$ selection. The efficiencies for $\mathcal{O}_{\text{FastBDT}} > 0.90$ [0.94] that are used in $B_s \rightarrow e^-\tau^+$ [$B_s \rightarrow \mu^-\tau^+$] are calculated to be $(69.3 \pm 1.7)\%$ [(64.7 \pm 1.7)%] for MC and $(69.9 \pm 1.6)\%$ [(65.6 \pm 1.7)%] for data. The uncertainty in the ratio of the data and MC efficiencies is assigned as the systematic uncertainty; these values are 3.3% for $B_s \rightarrow e^-\tau^+$ and 3.7% for $B_s \rightarrow \mu^-\tau^+$.

The semileptonic branching fraction of B_s is poorly known, so we estimate the systematic uncertainty of tagging from the data, using a control sample of $\bar{B}_s^0 \rightarrow D_s^+(X)\ell^-\bar{\nu}_\ell$ i.e., the $B_s \rightarrow \ell^-\tau^+$ mode is replaced by $B_s^0 \rightarrow D_s^-\ell^+\nu_\ell$. In this control sample study, the signal side $B_s^0 \rightarrow D_s^-\ell^+\nu_\ell$ is reconstructed using three D_s decay modes $D_s^- \rightarrow \phi(\rightarrow K^+K^-)\pi^-$, $K_S^0K^-$, and $K^{*0}(\rightarrow K^+\pi^-)K^-$. The tag-side $\bar{B}_s^0 \rightarrow D_s^+(X)\ell^-\bar{\nu}_\ell$ is reconstructed in the same way as for the $B_s \rightarrow \ell^-\tau^+$ analysis. We require the mass of the tag-side D_s meson candidate to be 1.96 GeV/ $c^2 < M_{D_s} < 1.98$ GeV/ c^2 . We also require the momentum of the tag-side lepton to be greater than 1.0 GeV/ c and $\mathcal{O}_{\text{FastBDT}}$ to be greater than 0.2. If there are multiple combinations in one event, the one with the highest FastBDT output is retained. We extract the signal by performing a one-dimensional unbinned fit to M_{D_s} on the signal side. We find the signal yields 34.3 ± 6.7 and 37.0 ± 6.8 for MC and data events, respectively, which are consistent within the uncertainty. These yields are approximately proportional to the square of the tagging efficiency including the branching fraction of semi-leptonic B_s decay to D_s , so we take half the uncertainty on the yields to be the systematic uncertainty from the tag side reconstruction. Taking into account additional contributions due to different D_s reconstruction and FastBDT selection in this control sample study, we assign 15.0% as the systematic uncertainty from the tag side reconstruction. This uncertainty includes the contribution of the uncertainty on the branching fraction of the semi-leptonic B_s decay to D_s as well as the effect of the reconstruction and selection on D_s and ℓ .

Other systematic uncertainties arise from the signal-side leptons ℓ_1 and ℓ_2 . The systematic uncertainty due to charged track reconstruction is estimated to be 0.35% per track by using the partially reconstructed $D^{*-} \rightarrow \bar{D}^0\pi^-$, $\bar{D}^0 \rightarrow \pi^-\pi^+K_S^0$ and $K_S^0 \rightarrow \pi^+\pi^-$ events [26]. The systematic uncertainties due to lepton identification are 4.3% and 3.5% for $B_s \rightarrow e^-\tau^+$ and $B_s \rightarrow \mu^-\tau^+$ decay modes, respectively. The systematic uncertainties due to the τ decay branching fractions are 0.2% [18].

Table 1: Estimated fractional systematic errors(%)

Source	$B_s \rightarrow e^- \tau^+$	$B_s \rightarrow \mu^- \tau^+$
$\overline{B}_s^0 \rightarrow D_s^+ \ell^- \overline{\nu}_\ell$ tag	15.0	15.0
FastBDT selection	3.3	3.7
Lepton ID	4.3	3.5
Tracking	0.7	0.7
$\tau \rightarrow \ell \nu_\tau \overline{\nu}_\ell$ branching fraction	0.2	0.2
Number of B_s	16.1	16.1
Total	22.7	22.6

In addition, the systematic uncertainty due to B_s meson counting is estimated as 16.1%. The total systematic uncertainty is taken as the sum in quadrature of all individual contributions.

5 Results and Summary

In the signal region, we find three events for $B_s \rightarrow e^- \tau^+$ and one event for $B_s \rightarrow \mu^- \tau^+$, as shown in Figure 5. The expected number of background events in the signal region, $N_{\text{bkg}}^{\text{exp}}$, is estimated from the number of events in the sideband, scaled by the ratio of events in the signal region and sideband without the $\mathcal{O}_{\text{FastBDT}}$ selection as determined from MC simulation. Here, the sideband is defined as $p_1^* \in [1.9, 2.1]$ GeV/ c and $p_1^* \in [2.7, 3.0]$ GeV/ c . We find $N_{\text{bkg}}^{\text{exp}} = 0.68 \pm 0.69$ for $B_s \rightarrow e^- \tau^+$ and $N_{\text{bkg}}^{\text{exp}} = 0.77 \pm 0.78$ for $B_s \rightarrow \mu^- \tau^+$. The number of observed events in the electron mode is larger but not inconsistent with the expected number, and the probability of obtaining three or more events with $N_{\text{bkg}}^{\text{exp}} = 0.68 \pm 0.69$ is 7.3%. From the p_1^* distribution for the $e^- \tau^+$ mode, we conclude that the observed events are likely to be background. Thus we calculate an upper limit on the branching fraction.

Table 2: Efficiency (ϵ), expected background events ($N_{\text{bkg}}^{\text{exp}}$), observed events (N_{obs}) and the 90% CL upper limits on \mathcal{B} and $f_s \times \mathcal{B}$

	ϵ (%)	$N_{\text{bkg}}^{\text{exp}}$	N_{obs}	\mathcal{B} ($\times 10^{-4}$)	$f_s \times \mathcal{B}$ ($\times 10^{-4}$)
$B_s \rightarrow e^- \tau^+$	0.0312 ± 0.0071	0.68 ± 0.69	3	< 14.1	< 5.5
$B_s \rightarrow \mu^- \tau^+$	0.0303 ± 0.0068	0.77 ± 0.78	1	< 7.3	< 2.9

To calculate this limit, we use the POLE program [27, 28] with the relation $\mathcal{B} = (N_{\text{obs}} - N_{\text{bkg}}^{\text{exp}})/(N_{B_s} \times \epsilon_{\text{sig}})$, where N_{obs} is the number of the observed events, N_{B_s} is the number of B_s mesons in the data $(16.6 \pm 2.7) \times 10^6$, and ϵ_{sig} is the signal

efficiency including the branching fraction of τ . The uncertainties on $N_{\text{bkg}}^{\text{exp}}$, N_{B_s} , and ϵ_{sig} are taken into account in the upper limit estimation. Since the uncertainty in f_s is significant, we report the upper limit not only on the branching fraction but also on $f_s \times \mathcal{B}(B_s \rightarrow \ell^- \tau^+)$. Table 2 summarizes the results, including the upper limit.

To summarize, we have searched for the decays $B_s^0 \rightarrow \ell^\mp \tau^\pm$ using the Belle data sample of 121 fb^{-1} collected at the $\Upsilon(5S)$ resonance. From the observed signal yields, we set upper limits

$$\begin{aligned}\mathcal{B}(B_s^0 \rightarrow e^\mp \tau^\pm) &< 14.1 \times 10^{-4} \\ \mathcal{B}(B_s^0 \rightarrow \mu^\mp \tau^\pm) &< 7.3 \times 10^{-4}\end{aligned}$$

at 90% confidence level. Our limit on the $B_s^0 \rightarrow e^\mp \tau^\pm$ decay rate is the first such limit reported. The sensitivity to these modes can be improved in the future with the Belle II experiment, which could collect a much larger data sample at the $\Upsilon(5S)$ resonance, and apply enhanced analysis techniques such as full reconstruction of the tag \bar{B}_s^0 [29].

Acknowledgments

This work, based on data collected using the Belle detector, which was operated until June 2010, was supported by the Ministry of Education, Culture, Sports, Science, and Technology (MEXT) of Japan, the Japan Society for the Promotion of Science (JSPS), and the Tau-Lepton Physics Research Center of Nagoya University; the Australian Research Council including grants DP180102629, DP170102389, DP170102204, DE220100462, DP150103061, FT130100303; Austrian Federal Ministry of Education, Science and Research (FWF) and FWF Austrian Science Fund No. P 31361-N36; the National Natural Science Foundation of China under Contracts No. 11675166, No. 11705209; No. 11975076; No. 12135005; No. 12175041; No. 12161141008; Key Research Program of Frontier Sciences, Chinese Academy of Sciences (CAS), Grant No. QYZDJ-SSW-SLH011; the Ministry of Education, Youth and Sports of the Czech Republic under Contract No. LTT17020; the Czech Science Foundation Grant No. 22-18469S; Horizon 2020 ERC Advanced Grant No. 884719 and ERC Starting Grant No. 947006 ‘‘InterLeptons’’ (European Union); the Carl Zeiss Foundation, the Deutsche Forschungsgemeinschaft, the Excellence Cluster Universe, and the VolkswagenStiftung; the Department of Atomic Energy (Project Identification No. RTI 4002) and the Department of Science and Technology of India; the Istituto Nazionale di Fisica Nucleare of Italy; National Research Foundation (NRF) of Korea Grant Nos. 2016R1D1A1B02012900, 2018R1A2B3003643, 2018R1A6A1A06024970, RS202200197659, 2019R1I1A3A01058933, 2021R1A6A1A-03043957, 2021R1F1A1060423, 2021R1F1A1064008, 2022R1A2C1003993; Radiation Science Research Institute, Foreign Large-size Research Facility Application Supporting project, the Global Science Experimental Data Hub Center of the Korea

Institute of Science and Technology Information and KREONET/GLORIAD; the Polish Ministry of Science and Higher Education and the National Science Center; the Ministry of Science and Higher Education of the Russian Federation, Agreement 14.W03.31.0026, and the HSE University Basic Research Program, Moscow; University of Tabuk research grants S-1440-0321, S-0256-1438, and S-0280-1439 (Saudi Arabia); the Slovenian Research Agency Grant Nos. J1-9124 and P1-0135; Ikerbasque, Basque Foundation for Science, Spain; the Swiss National Science Foundation; the Ministry of Education and the Ministry of Science and Technology of Taiwan; and the United States Department of Energy and the National Science Foundation. These acknowledgements are not to be interpreted as an endorsement of any statement made by any of our institutes, funding agencies, governments, or their representatives. We thank the KEKB group for the excellent operation of the accelerator; the KEK cryogenics group for the efficient operation of the solenoid; and the KEK computer group and the Pacific Northwest National Laboratory (PNNL) Environmental Molecular Sciences Laboratory (EMSL) computing group for strong computing support; and the National Institute of Informatics, and Science Information NETWORK 6 (SINET6) for valuable network support. S.N. is supported by JSPS KAKENHI grant JP17K05474.

References

- [1] S. Fukuda *et al.* (Super-Kamiokande Collaboration), *Phys. Rev. Lett.* **85** (2000), 3999–4003, arXiv:hep-ex/0009001 [hep-ex].
- [2] D. London and J. Matias, *Annual Review of Nuclear and Particle Science* (2022), 72, page 37–68, arXiv:2110.13270 [hep-ph]
- [3] U. Egede, S. Nishida, M. Patel, M. Schune, 72, page 283–305, arXiv:2205.05222v1 [hep-ex]
- [4] A. Crivellin *et al.*, *Phys. Rev. D* **92** (2015) 054013, arXiv:1504.07928.
- [5] A. D. Smirnov, *Mod. Phys. Lett. A* **33** (2018) 1850019, arXiv:1801.02895.
- [6] I. de Medeiros Varzielas and G. Hiller, Clues for flavor from rare lepton and quark decays, *JHEP* **6** (2015) 72, arXiv:1503.01084.
- [7] R. Aaij *et al.* (LHCb Collaboration), *Phys. Rev. Lett.* **123**, 211801 (2019), doi:10.1103/PhysRevLett.123.211801 [arXiv:1905.06614 [hep-ex]].
- [8] S. Kurokawa and E. Kikutani, *Nucl. Instrum. Methods Phys. Res. Sect. A* **499**, 1 (2003)
- [9] T. Abe *et al.*, *Prog. Theor. Exp. Phys.* **2013**, 03A001 (2013)
- [10] A. Abashian *et al.* (Belle Collaboration), *Nucl. Instrum. Methods Phys. Res. Sect. A* **479**, 117 (2002)
- [11] J. Brodzicka *et al.*, *Prog. Theor. Exp. Phys.* **2012**, 04D001 (2012)

- [12] D.J. Lange, *Nucl. Instrum. Methods Phys. Res. Sect. A* **462**, 152 (2001).
- [13] R. Brun *et al.*, GEANT 3.21, CERN Report DD/EE/84-1, 1984.
- [14] M. Gelb *et al.*, *Comput. Softw. Big Sci.* **2**, 9 (2018).
- [15] T. Kuhr *et al.* (Belle II Framework Software Group), *Comput. Softw. Big Sci.* **3**, 1 (2019).
- [16] Belle II Collaboration, Belle II Analysis Software Framework (basf2), <https://doi.org/10.5281/zenodo.5574115>.
- [17] S. Esen *et al.* (Belle), *Phys. Rev. D* **87**, 031101 (2013), doi:10.1103/PhysRevD.87.031101 [arXiv:1208.0323 [hep-ex]].
- [18] R. L. Workman *et al.* (Particle Data Group), *PTEP* **2022**, 083C01 (2022) doi:10.1093/ptep/ptac097
- [19] H. Nakano *et al.* (Belle Collaboration) *Phys. Rev. D* **97**, 092003 (2018)
- [20] A. Abashian *et al.*, *Nucl. Instrum. Methods Phys. Res. Sec A* **491**,69 (2002).
- [21] K. Hanagaki, H. Kakuno, H. Ikeda, T. Iijima and T. Tsukamoto, *Nucl. Instrum. Methods Phys. Res., Sec. A* **485**, 490 (2002).
- [22] T. Keck, *Comput Softw Big Sci* **1**, 2 (2017). <https://doi.org/10.1007/s41781-017-0002-8>
- [23] G. C. Fox and S. Wolfram, *Phys. Rev. Lett.* **41**, 1581 (1978)
- [24] S.H. Lee *et al.* (Belle Collaboration), *Phys. Rev. Lett.* **91**, 261801 (2003)
- [25] G. Punzi, Sensitivity of searches for new signals and its optimization, arXiv:physics/0308063v2
- [26] S. Ryu *et al.* (Belle Collaboration), *Phys. Rev. D* **89**, 072009 (2014).
- [27] J. Conrad, O. Botner, A. Hallgren, and C. P´erez de los Heros, *Phys. Rev. D* **67**, 012002 (2003)
- [28] <https://github.com/ftegenfe/polepp> (updated version of the POLE program).
- [29] T. Keck *et al.*, arXiv:1807.08680 [hep-ex]
- [30] T. Pang *et al.* (Belle Collaboration), Search for the decay $B_s^0 \rightarrow \eta' K_S^0$, arXiv:2201.01851 [hep-ex].
- [31] G.J. Feldman and R.D. Cousins, *Phys. Rev. D* **57**, 3873 (1998).
- [32] E. Nakano, *Nucl. Instrum. Methods Phys. Res. Sect. A* **494**, 402 (2002).